AMSE JOURNALS-AMSE IIETA publication-2017-Series: Modelling B; Vol. 86; N°2; pp 517-534
Submitted Mar. 27, 2017; Revised May 22, 2017; Accepted May 31, 2017

Experimental Analysis and Numerical Simulation on Impact Response of Sand-filled Aluminium Honeycomb Sandwich Structure

*Weiming Luo, **Shaoqing Shi, ***Jianhu Sun, ****Yuzheng Lv

*Department of Civil Engineering, Logistical Engineering University, Chongqing 401311, China (lwmofficial@163.com)

**Department of Civil Engineering, Logistical Engineering University, Chongqing 401311, China

***Department of Civil Engineering, Logistical Engineering University, Chongqing 401311, China

****Beijing Canbao Institute of Architectural Design, Beijing 100000, China

Abstract

This paper proposes a sand-filled aluminium honeycomb sandwich structure for protective structures. Based on the results of the theoretical analysis, the author conducted a drop weight impact experiment was conducted on several specimens, seeking to obtain the data on impact load, impactor displacement and structure deflection, and observe damage modes of structures at different impact energies. Then, the LS-DYNA was employed to validate the simulation model. The experiment results demonstrate that the strength and stiffness of the structures were improved by sand-filling under the impact of low energy level, especially for the structures with softer honeycomb core. With the same mass, honeycomb core with smaller cell size and lower height is preferable at low energy level. Localized structural deflection and damaged area were also observed under impact of high-energy level when the core height reached a fixed value. The model of numerical simulation was validated with the experimental results, which can be used in further research.

Key words

Aluminium honeycomb, Sand-filled, Impact response, Low velocity.

1. Introduction

Thanks to good mechanical properties and strong energy adsorption, aluminium honeycomb sandwich structures [1] have been extensively utilized in aerospace, protection, automobile, shipping and other fields. As a research hotspot, sandwich structure performance is mainly improved in three ways. The first option is to use lightweight and high-strength materials as the face sheets of the sandwich structure. For instance, G. Belingardi [2] carried out four-point bending experiments to examine the fatigue damages of a composite sandwich beam, which consists of carbon fibre face sheets and an aluminium honeycomb core. Abdullah Akatay et. al. [3] attempted to improve the impact resistance of the sandwich structure by integrating glass fibre-reinforced epoxy resin face sheets with an aluminium honeycomb core. The second approach is to adopt different cores, ranging from honeycomb core, lattice core [4-5], cork core [6], foam core [7] and so on. The suitable materials of honeycomb core include aluminium, polypropylene, Nomex [8] and paper [9], etc. The third way is to utilize multiple forms like composition, filling and enhancement. For example, Bin Han [10] combined aluminium corrugations and trapezoidal aluminium honeycomb blocks into a novel sandwich structure, and investigated the performance of the hybrid structure under quasi-static out-of-plane compression. Through theoretical and experimental analysis, it is observed that the structure has a much greater strength and energy absorption capacity than those of the sandwich specimens having empty corrugated core and honeycomb core combined. Foam filling is also a frequently reported method. Hozhabr Mozafari et al. [11] filled the honeycomb core of sandwich structure with polyurethane foam, quantified the increment of energy absorption and impact resistance, and tested the effect of face sheets using woven composites with good shock resistance. Guoqi Zhang [5] studied the impact resistance and energy absorption of pyramidal lattice-cored sandwich structure filled with polyurethane foam under low-velocity impact, concluding that the foam-filled specimens have a shorter contact duration with the impactor and slight higher peak impact load than the unfilled specimens. To enhance the stiffness of soft honeycomb, Shanshan Shi [12] added orthogrid into the sandwich structure and performed three-point bending tests on the structure. The test results indicate that the addition improved the mechanical properties of the structure. Shi [13] and his team also used short Kevlar fibre to enhance the strength of interface between carbon fibre face sheets and aluminium honeycomb core, and verified the feasibility and effectiveness of the enhancement through a three-point bending test. It is demonstrated that the

resulting composite structure boasts a tough interface, high peak load and good energy absorption.

In light of the above, this paper puts forward a brand-new sand-filled aluminium honeycomb sandwich structure (Figure 1), and carries out a series of tests on Dynatup 9250HV (Instron) to investigate the impact response of the structure at low velocity. The time-history curves on force and displacement under impact were recorded during the tests, and the damage modes of all specimens were compared after the tests. Based on the finite element method (FEM) and the smoothed-particle hydrodynamics (SPH) method, the author performed numerical simulations, and compared the simulation results with the test results, seeking to validate the proposed structure.

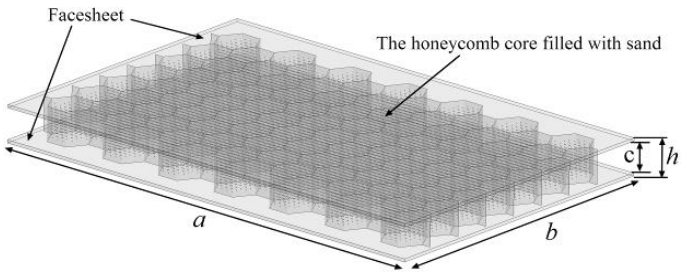

Fig.1. Sand-Filled Aluminium Honeycomb Sandwich Structure

2. Theoretical Analysis

Due to the periodicity of the constituent cells, the mechanical properties of the honeycomb can be deduced based on those of a minor portion in the whole structure [14]. In this research, a Y-shaped cross-section is taken as the object (Figure 2).

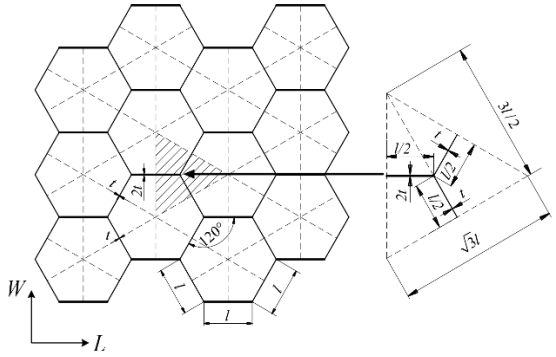

Fig.2. Y-shaped cross-sectional model of honeycomb [17]

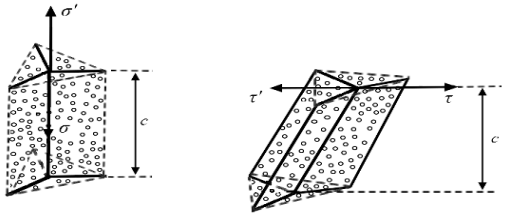

Fig.3. Stress analysis of the Y-shaped cross-sectional model

When the sand-filled aluminium honeycomb sandwich structure is subjected to out-of-plane impact, the impact area mainly suffers from compressive deformation. As the impact energy continues to rise, shear deformation will also occur around the impact area. At a high level of impact energy, the impact area will exhibit both compressive and shear deformations. Hence, force decomposition was conducted to analyse the stress state of the Y-shaped cross-sectional model (Figure 3). When the model is in elastic state, the stress resistances σ' and τ' to compressive stress and shear stress can be divided into:

$$\begin{cases} \sigma' = \alpha\left(\sigma_{he} + \sigma_s\right) \\ \tau' = \beta\left(\tau_{he} + \tau_s\right) \end{cases} \tag{1}$$

where σ_{he} and τhe are the elastic compressive stress and the elastic shear stress of aluminium honeycomb, respectively; σ_s and τ_s are the compressive stress and shear stress applied by sand, respectively; α and β are the interaction coefficients of aluminium honeycomb and sand, respectively. Thus, the axial elastic yield load of monolithic aluminium foil can be determined by the second-order moment of inertia and cell length l [15]:

$$P_{crit} = \frac{KE_h}{(1-\nu_h^2)}\frac{t^3}{l} \tag{2}$$

where the constant K is an end constraint factor set to 5.73 for hexagonal honeycomb; E_h and ν_h are the elastic modulus and Poisson's ratio of aluminium alloy, respectively; t is the thickness of the aluminium alloy foil. According to Figure 2, the area of the Y-shaped cross-sectional model can be calculated as:

$$A_h = \sqrt{3}l \times (3l/2)/2 = 3\sqrt{3}l^2/4 \tag{3}$$

Therefore, the elastic yield load of the model equals the sum of the loads borne by the individual cell walls:

$$\sigma_{he} = \frac{(8P_{crit} + 2P_{crit})/2}{A_h} = \frac{5KE_h t^3 / l}{3\sqrt{3}l^2(1-\nu_h^2)/4} = 22.05 \times \frac{E_h (t/l)^3}{(1-\nu_h^2)}$$

(4)

Based on the mechanical properties of dry sand, the σ' in equation (1) can be equivalent to:

$$\sigma' = \frac{22.05\alpha E_h (t/l)^3}{(1-\nu_h^2)} + \alpha\sigma_{cp} \tan^2(45° + \frac{\varphi_s}{2}) \tag{5}$$

where σ_{cp} is the confining stress on sand; φ_s is the internal friction angle of sand. For the geometrical feature of the honeycomb, τ_{he} can be decomposed along the two directions of L and W:

$$\begin{cases} \tau_L = \dfrac{CE_h (t/l)^3}{(1-\nu_h^2)\cos\theta} \\ \tau_W = \dfrac{CE_h (t/l)^3}{(1-\nu_h^2)(1+\sin\theta)} \end{cases}$$

(6)

where C is a constant; θ is the angle between the inclined cell wall and the W direction. When the model is in plastic state, the σ_{he} and τ_{he} in equation (1) should be changed into plastic compressive stress σ_{hp} and plastic shear stress τ_{hp}, and σ_{hp} can be approximated as:

$$\sigma_{hp} = 6.6\sigma_y (t/l)^{\frac{5}{3}}$$

(7)

where σ_y is the yield strength of aluminium alloy. Based on the model of average static plastic compressive stress and Cowper-Symonds constitutive model, Guowei Zhao [16] built a new

theoretical model, in which the enhanced strain effect and the average plastic compressive stress are expressed as follows:

$$\sigma_{hp} = k\sigma_y \left(\frac{t}{l}\right)^{\frac{3}{2}} \left[1+\left(\frac{\upsilon}{1.68Cl}\right)^{\frac{1}{p}}\right]\left(1+\frac{tE_p}{2.83\sigma_y \times \sqrt[3]{t^2 l}}\right) \tag{8}$$

where k is a constant; v is the impact velocity; C and p are the coefficients of strain rate sensitivity; E_p is the plastic hardening modulus. It can be inferred from above analysis that the impact response of the of sand-filled aluminium honeycomb sandwich structure is under the influence of honeycomb material, geometric parameters, sand properties, packing density, sand-honeycomb interaction, impact energy and impactor velocity. The theoretical analysis lays the basis for variable setting in drop weight impact experiment.

3. Drop Weight Impact Experiment

3.1 Materials and Specimens

The drop weight impact experiment was conducted in reference to the ASTM D7136/D7136M, 2005. Based on the theoretical analysis, the multivariate analysis was simplified into single variable analysis by the one-variable-at-a-time method. For all the specimens, the face sheets were made of 1mm-thick AL-5052-H32, and the cores were made of 0.04mm-thick AL3003-H18 foil. The material properties of AL-5052-H32 and AL3003-H18 are listed in Table 1. The specimens were classified into four types: A, B, B1 and B2. The relative density of honeycomb can be calculated as follows:

$$\frac{\rho_h}{\rho_b} = \frac{2lt \cdot c}{A_h \cdot c} = \frac{2lt}{3\sqrt{3}l^2/4} = \frac{8\sqrt{3}}{9}\frac{t}{l} \tag{9}$$

where p_h is the density of the honeycomb; p_b is the density of the aluminium alloy. With the cell size selected as the single variable, type A must differ from type B in cell size, but agree with the latter on mass. Thus, the cell length l and cell height c of type A were set to 3.5mm and 5mm, respectively, while those of type B were made as 7mm and 10mm, respectively. The core height

of types B, B1 and B2 was configured as 10mm, 15mm, and 20mm, respectively. All the specimens are displayed in Figure 4.

To examine the effect of sand-filling on the structure, the specimens were divided again into two groups: those with sand-filled cores and those with empty cores. The sand was filled into the cores via natural accumulation, so that all the specimens had the same packing density. The *L* direction was taken as the length of the specimens, for the shear strength in *L* direction was about twice of that in *W* direction of hexagonal honeycomb.

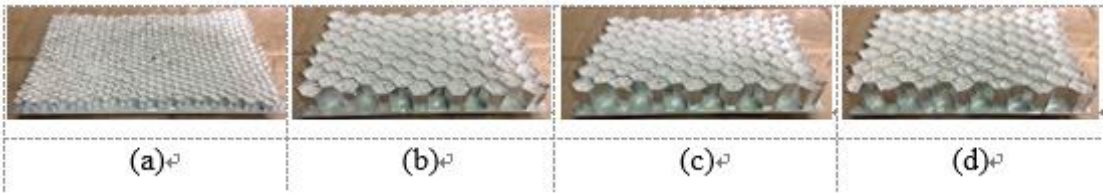

Fig.4. Specimens (a) Type A; (b) Type B; (c) Type B1; (d) Type B2

Tab.1. Mechanical properties of base materials for face sheets and honeycomb core

Base material	Density ρ_s (g/cm^3)	Elastic modulus E_e (GPa)	Tangent modulus E_t (GPa)	Poisson ratio v_s	Yielding strength σ_y (MPa)	Ultimate strength σ_u (MPa)
Al-3003-H18	2.73	68.9	6.9	0.33	186	200
Al-5052-H32	2.68	70.3	7.1	0.33	193	228

3.2 Methods

The drop weight impact experiment was performed on Dynatup 9250HV (Instron). The mass of the impactor and the weight totalled 10.09kg, and the diameter of the hemispherical head impactor was 12.7 mm with a hemispherical head. The free-fall height was automatically adjusted by the motor-driven lift rail based on the impact energy, and the data were automatically collected by the Impulse Data Acquisition software. According to the ASTM D7136/D7136M, 2005, the specimen was clamped on a 150mm×100mm support with a 125 mm×75 mm rectangular hole at the support center. During the loading process, the load and displacement were collected respectively by the force sensor and displacement sensor in the impactor. The experimental setup is shown in Figure 5.

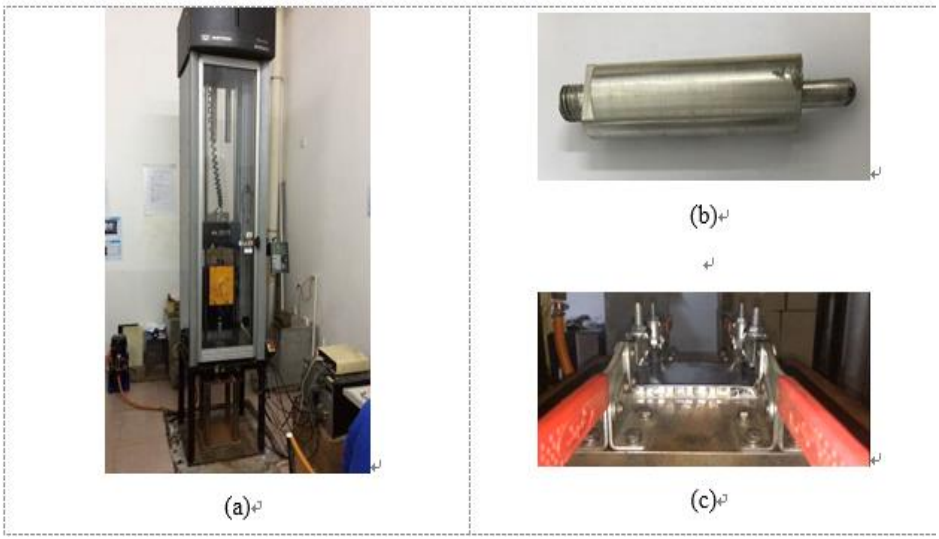

Fig.5. Experimental setup: (a) Dynatup 9250 HV; (b) impactor; (c) clamp

4 Numerical Simulation

4.1 Finite-element Model

The numerical simulation was carried out using the explicit double precision version of LS-DYNA. As shown in Figure 6(a), the face sheets, core, impactor and support were modelled as finite elements, denoted as SHELL163. The shell thickness was configured by the keyword of SECTION_SHELL in line with the specimen size. The element sizes were meshed into 1 mm to ensure calculation accuracy and control the computing time. In view of the possible large deformations in honeycomb core, the number of integration points through the shell thickness of the honeycomb was set to 5, aiming to prevent the hourglass problem resulted from single point integration. The impactor and support were regarded as rigid bodies, as they underwent no plastic deformation during the loading process. Despite the insensitive strain rate effect of aluminium alloy, the material model PLASTIC_KINETIC was utilized to guarantee the accuracy of the constitutive model of aluminium alloy face sheets and honeycomb core. Considering the Cowper-Symonds strain rate effect, the constitutive model can be expressed as:

$$\frac{\sigma^d}{\sigma_0} = 1 + \left(\frac{\dot{\varepsilon}}{C}\right)^{1/p} \tag{10}$$

where σ^d is the dynamic flow stress at the strain rate; σ_0 is the static stress; C (6500 s-1) and p (4) are the strain rate sensitivity coefficients of aluminium alloy material. Moreover, the node group with sliding friction constraints was set to simulate the constraint of clamp; the

TIED_SURFACE_TO_SURFACE_FAILURE was used to simulate the contact between face sheets and core; the AUTOMATIC_SURFACE_TO_SURFACE_FAILURE was applied to the rest of contacts between each part; the impact velocity was defined by the keyword INITIAL_VELOCITY_GENERATION.

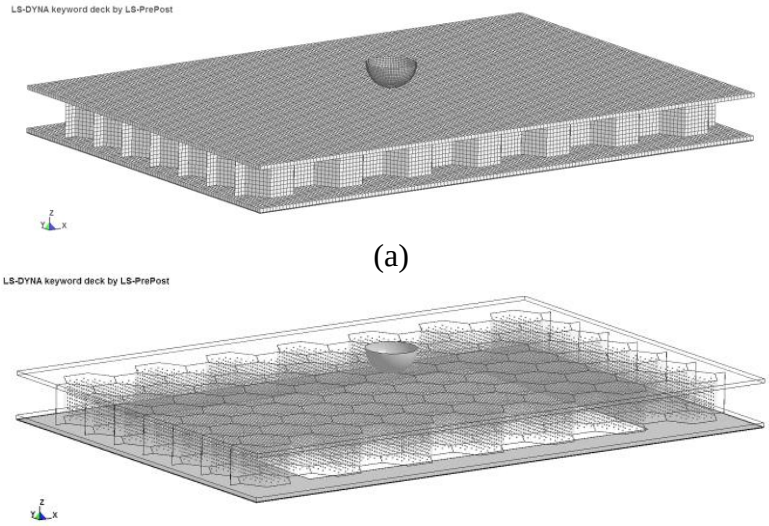

(a)

(b)

Fig.6. Model of the sand-filled aluminium honeycomb sandwich structure

(a) Finite-element models of impactor, structure and support; (b) SPH particles of sand in honeycomb.

4.2 SPH Model

Smoothed-particle hydrodynamics (SPH) is a meshless, particle-based computing technique for numerical simulation. Like the FEM, the SPH can effectively prevent mesh distortion under large deformations. Therefore, SPH particles are desirable tools to simulate the sand. The SOIL_AND_FOAM_FAILURE model works like a fluid in some ways, and applies only to such scenarios that the soil or foam is confined in a structure or the geometric boundaries are clearly defined (Figure 6(b)). The relationship between pressure and volume strain was used to describe the constitutive model of the sand under compression [17]. The SPH particles were generated by LS-PrePost program, and their parameters are listed in Table 2.

Tab.2. Material parameters in the LS-DYNA

Material model	Density ρ_s (g/cm^3)	Elastic modulus E (MPa)	Poisson ratio v(MPa)
RIGID-impactor	7.85	210	0.3

PLASTIC_KINETIC-facesheet	2.68	70.3	0.33
PLASTIC_KINETIC-core	2.73	68.9	0.33
Material model-sand	Density ρ_s (g/cm^3)	Shear modulus G (MPa)	Bulk modulus (MPa)
SOIL_AND_FOAM_FAILURE	1.8	63.8	1260

5 Results and Analysis

5.1 Impact Response

Four impact energies were used in the experiment to figure out how the sand-filled aluminium honeycomb sandwich structure responds to low velocity impact. The initial values were set to 25J, 50J, 100J and 150J, respectively. However, it is the final measured value (17J, 39J, 83J and 119J), always lower than initial value, that determines the impact energy. For comparative analysis, the 17J and 39J were classified as low energy level, while the 83J and 119J were classified as high energy level. In the low energy level, the author probed into the effect of cell size on impact response by comparing types A and B; in the high energy level, the author explored the effect of core height on impact response by comparing types B, B1 and B2.

According to the impact response in low energy level (Figure 7), both the peak load and the final displacement increased with the impact energy for all specimens. The sand-filled specimens had higher peak load and shorter final displacement than the empty-core counterparts. In the meantime, the force-displacement curves of the sand-filled specimens were smoother than the somewhat turbulent curves of empty-core specimens. The turbulence was particularly prominent in the curves of empty-core type B specimen when the impact load reached the yield strength of the honeycomb core. The empty-core specimen also exhibited prominent bending deflections, resulting in a certain decline in the Y-value of the curves. After sand-filling, type B specimen featured greater peak load increment and displacement decrement in force-displacement curves than type A specimen. This is because type B specimen has larger cells with lower compressive strength. In other words, the core of type B specimen is softer than that of type A specimen. Therefore, sand-filling has more obvious strength enhancement effect in type B specimen than type A specimen. It should be mentioned that the two types of specimens differed slightly in the peak load and final displacement in the force-displacement curves after sand-filling. As a result, it

is better to select a smaller and shorter core for the sand-filled aluminium honeycomb sandwich structure under the impact of low energy level.

According to the impact response in high energy level (Figure 8), the peak load grew but the final displacement shortened with the increase in the impact energy. Due to the yield of honeycomb, there was a small peak (1.5 kN~2.5 kN) in the force-displacement curve of each empty-core specimen at the initial phase (displacement: 6~8mm), which is shown as the red curves. In addition, the red curves in Figures 8(b), (d), (e) and (f) and the black curve in Figure 8(f) recorded a higher peak in the later phase of impact. Such a peak is attributable to the contact force between the coarse parts of the impactor and the upper face sheet, which prevented further penetration after the specimen was fully penetrated. Therefore, this peak value should not be taken into account in the dynamic response analysis. Overall, the impact load of the force-displacement curve could reach the peak more quickly, owing to the improved structural stiffness after sand-filling. Then, the load fluctuated and declined because of the interaction among impactor, honeycomb and sand, as shown in the black curves of Figures 8(c), (d), (e) and (f).

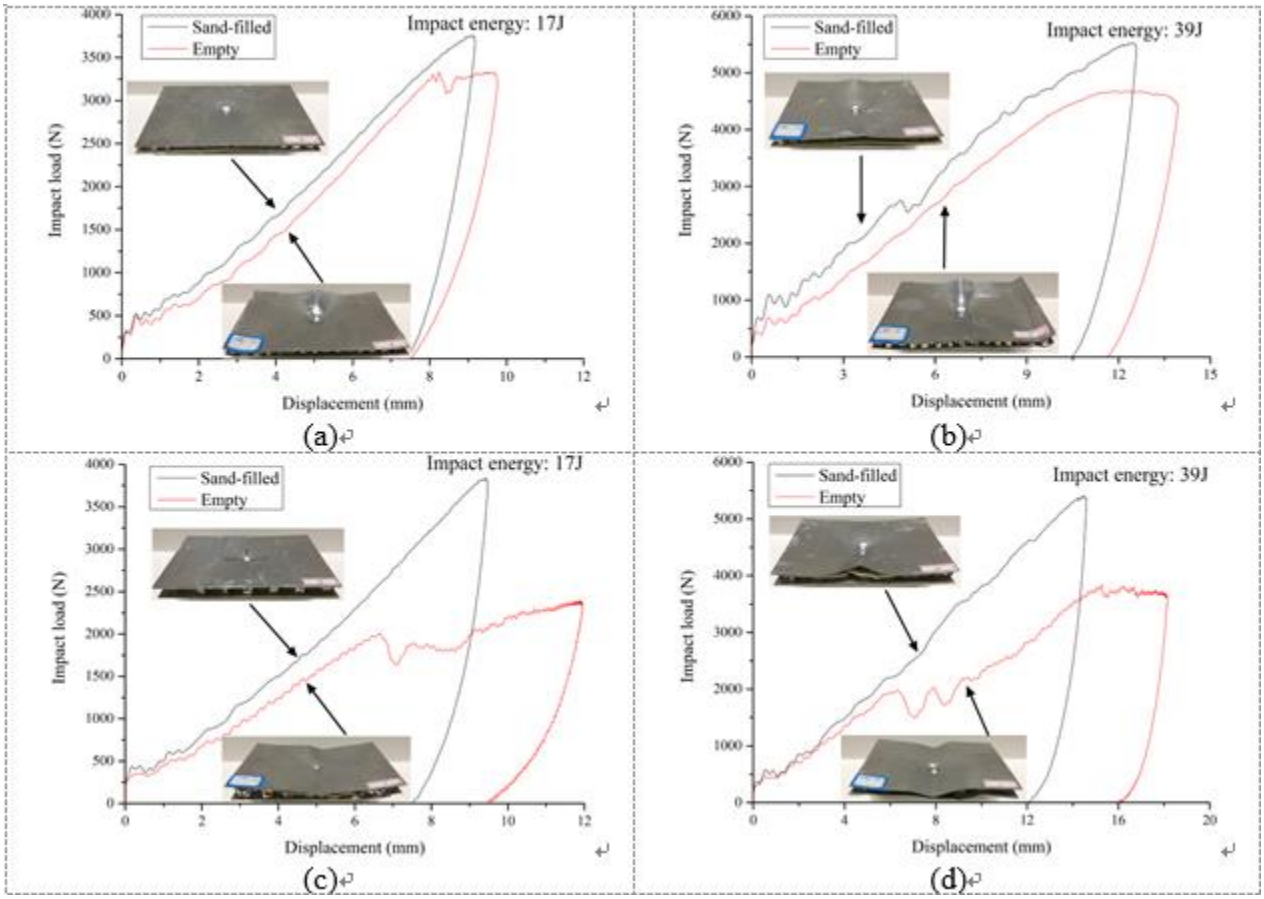

Fig.7. Impact response in low energy level: (a) type A at 17J; (b) type A at 39J; (a) type B at 17J; (b) type B at 39J.

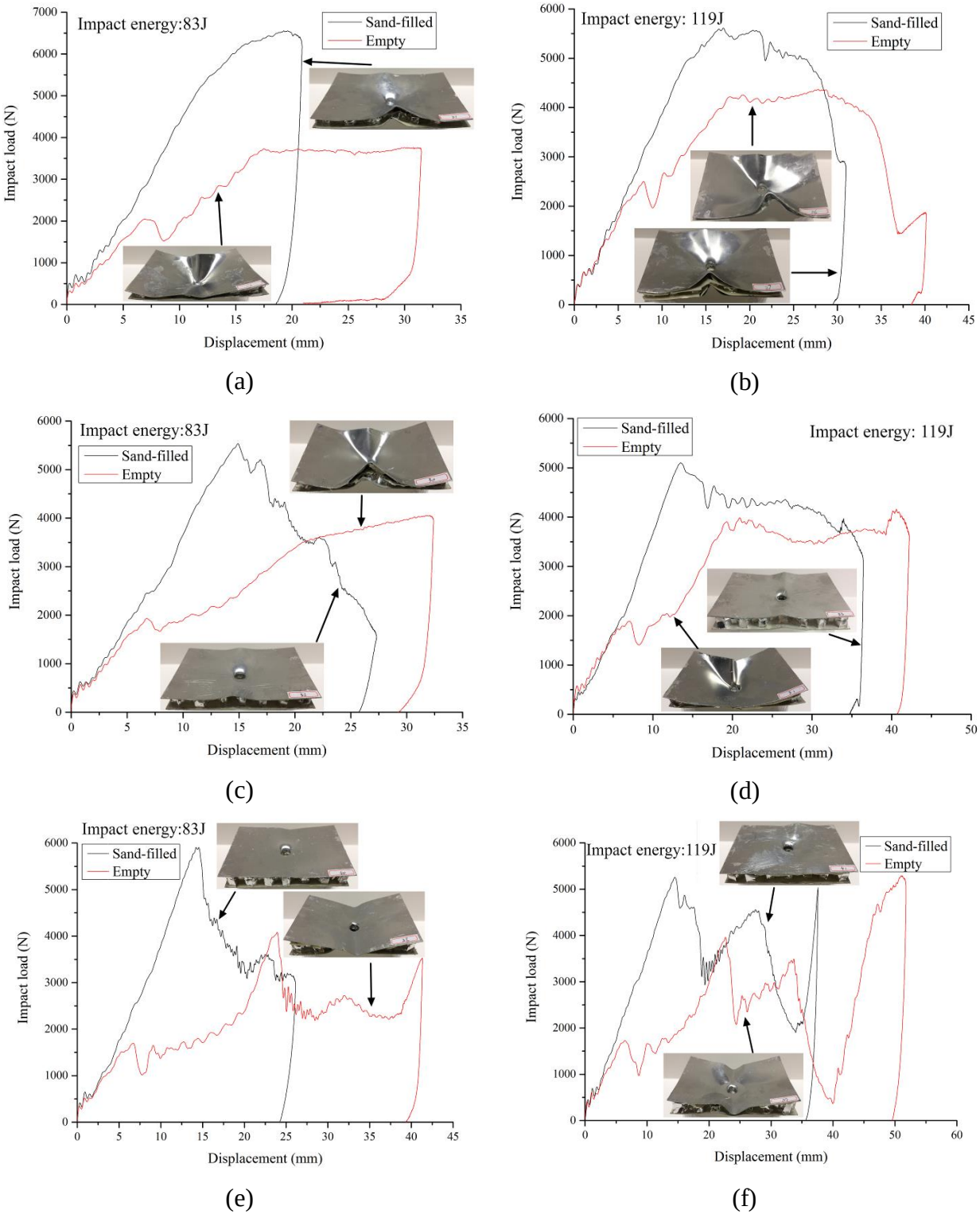

Fig.8. Impact response in high energy level: (a) type B at 83J; (b) type B at 119J; (c) type B1 at 83J; (d) type B1 at 119J; (e) type B2 at 83J; (f) type B2 at 119J

5.2 Variation Pattern of Peak Load, Displacement and Deflection

Figure 9(a) presents pronounced increase of peak load at low energy level (17J~39 J), but the increase slowed down in the transition (39J~83 J) from low energy level to high energy level. The trend is explained as follows. Under the impact of low energy level, the impactor only left a spherical dent on the upper face sheet, producing a small deflection of the structure. Hence, the peak load increased with the impact energy, but the increment diminished as the deflection expanded with some cracks on the upper face sheet. After reaching the high energy level (83J~119 J), the peak load declined as the structure was fully penetrated. It must be noted that the critical energy of full penetration should fall in the range of 83J~119J.

As can be seen from Figure 9(b), the final displacement of the impactor lengthened with the increase in impact energy, especially at the high energy level. The variation pattern is created by the structural deformation and destruction of face sheets and core. The final displacements shot up at the total penetration of the structures.

Based on the deflections of lower face sheets, it is observed that the structural deflection of most specimens increased linearly with the growth of impact energy at low energy level and the transition from the low energy level to the high energy level. In the high energy level, the deflection of sand-filled B1 and B2 specimens shown a decreasing trend (Figure 9(c)). By contrast, the deflection of type B specimen continued to increase linearly, although the cell size was the same with that of B1 and B2. The above phenomena reveal that the deflection of the sand-filled structure will decrease when the core height reaches a fixed value. Through the comparison between types B, B1 and B2 specimens, it is discovered that the damaged area was localized and shrunk to a hole at the centre of the face sheet.

Under the increasing impact energy, the damage started from the upper face sheet, propagated to the core, and spread to the lower face sheet. When the impact was only 17J, there was no damage on the structures except a small dent on the upper face sheet. At 39J, only the upper face sheet of empty-core type B specimen was penetrated, and cracks appeared on the upper face sheet in half of the specimens. Almost all of the specimens were fully penetrated at 119J.

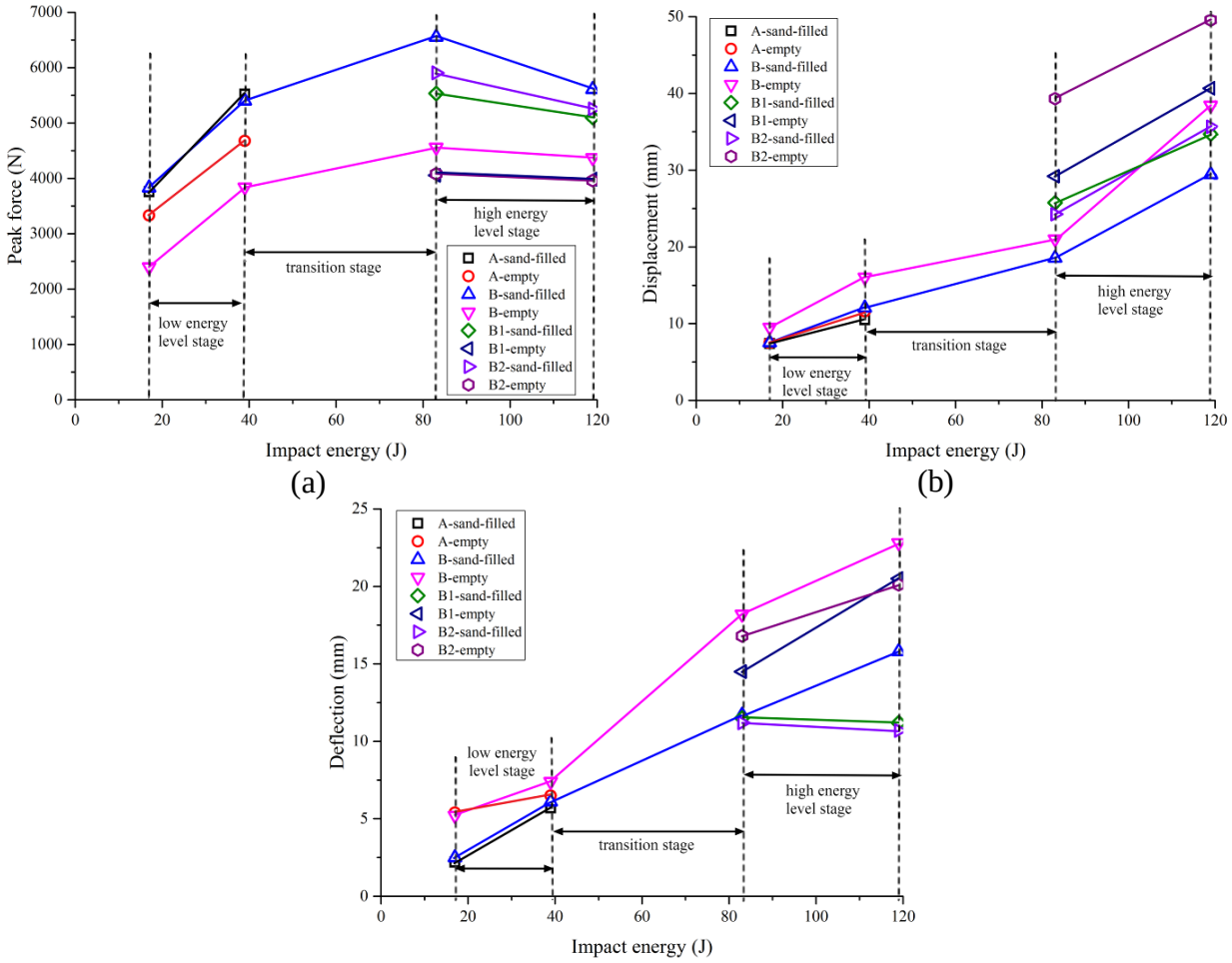

Fig.9. Variation pattern: (a) peak load; (b) displacement; (c) deflection

5.3 Verification of the Model

To validate of the numerical model, type B specimen was selected as the typical modelling object. As shown in Figure 10, the simulation results are in good agreement with the experimental results according to the time history curves of impact load. The results of the numerical simulation are slightly higher than those of the experimental results. The error of the peak load in red curve is smaller than those of black curve, indicating that the simulation results of empty-core specimens are more accurate than those of sand-filled specimens. Moreover, the damage modes of test specimens are consistent with the simulation results (Figure 11). For sand-filled specimens, the simulated deformation is smaller than the measured deformation. The small deviation may be caused by various factors, including model parameters, interaction between SPH particles and finite elements, and so on. These comparisons manifest that the proposed finite-element/SPH model can make reasonable predictions of the dynamic responses and damage modes of the structures under impact loads.

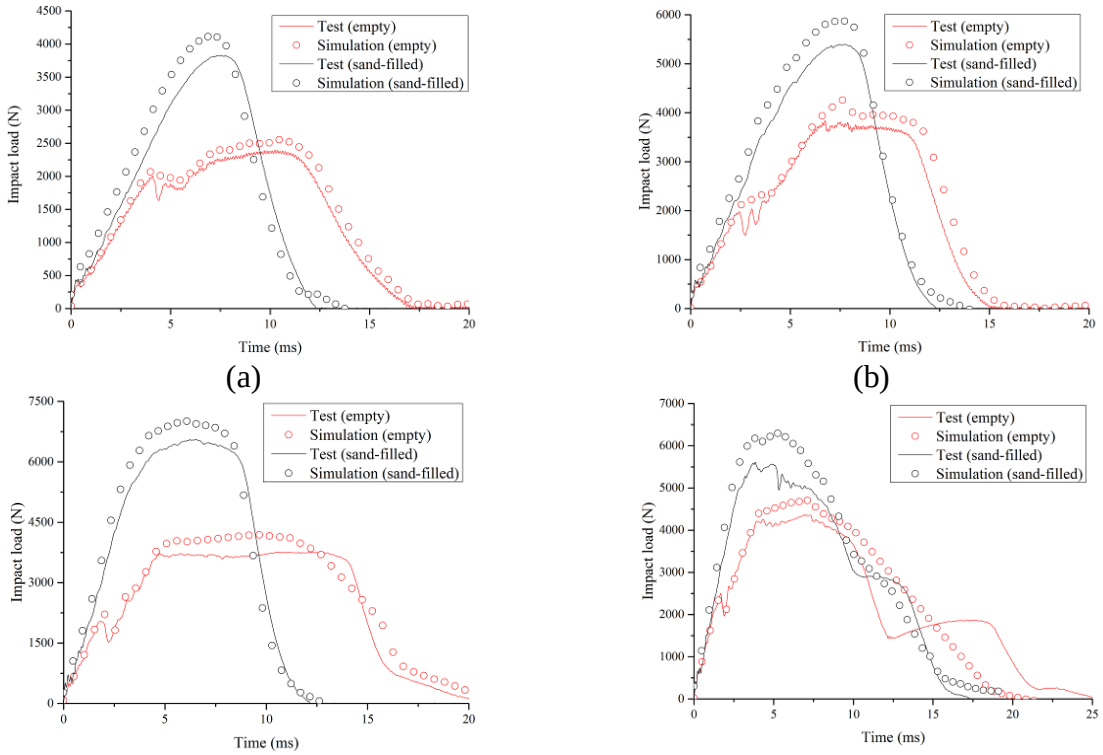

Fig.10. Time history curves of impact load: (a) 17J; (b) 39J; (c) 83J; (d) 119J

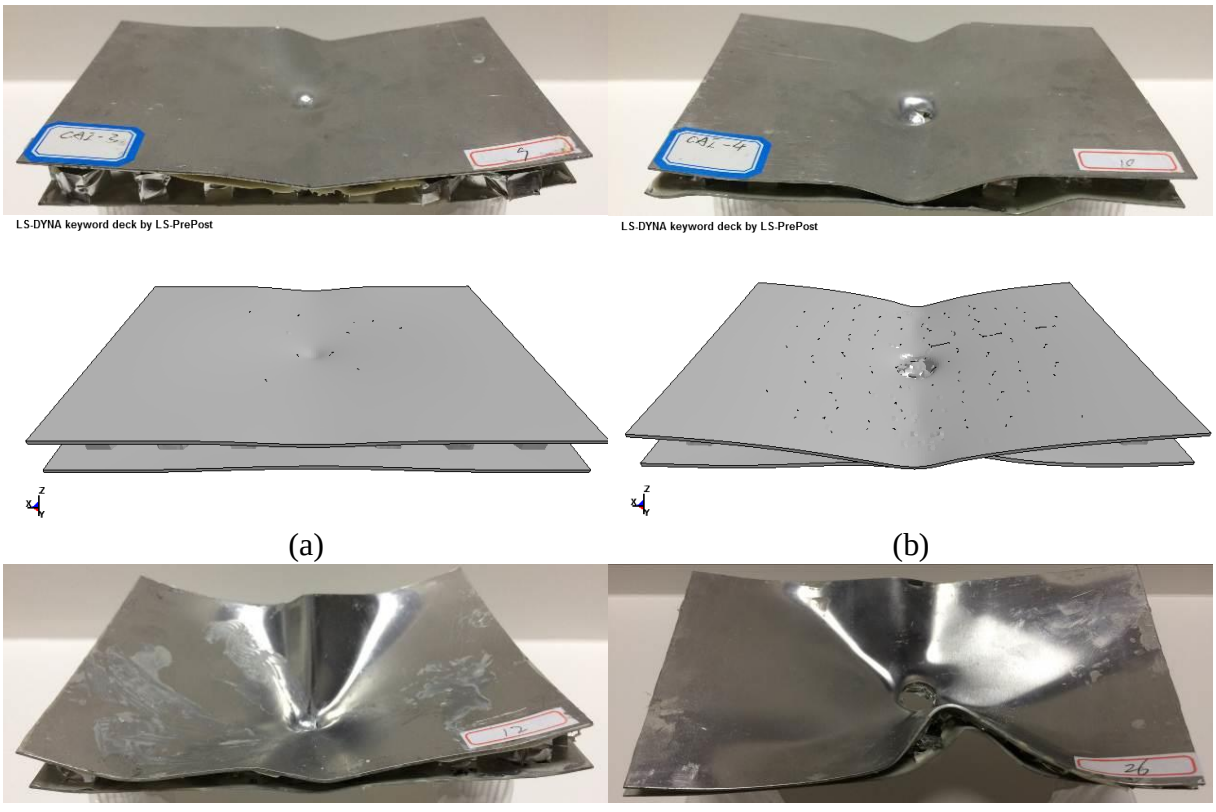

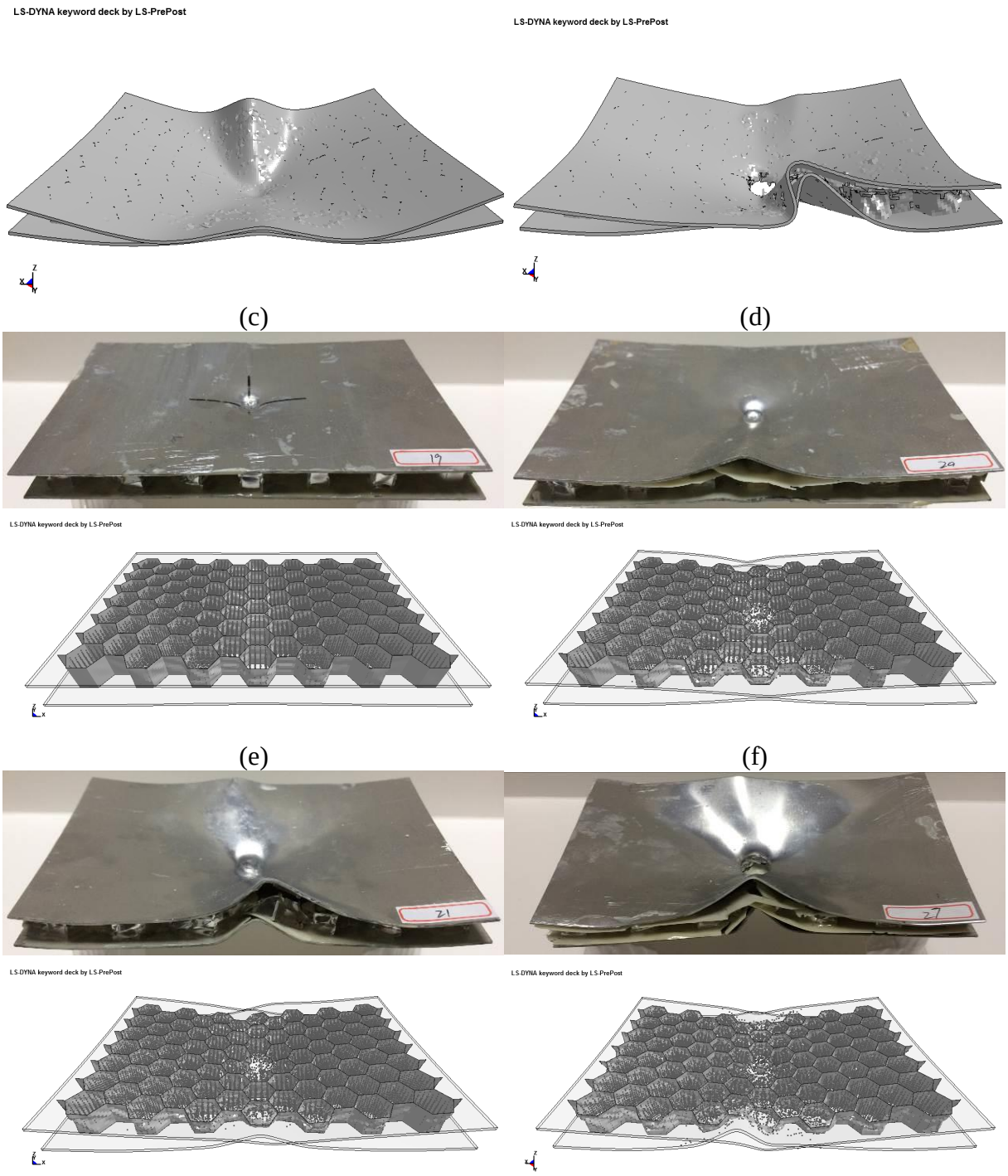

Fig.11. Comparison between test results and simulation results: (a) B-S-17J; (b) B-E-17J; (c) B-S-39J; (d) B-E-39J; (e) B-S-83J; (f) B-E-83J; (g) B-S-119J; (h) B-E-119J. (Postfix -S denotes the sand-filled specimens; Postfix -E denotes the empty-core specimens.)

Conclusions

This paper explores how the sand-filled aluminium honeycomb sandwich structure responds to low-velocity impact. Through theoretical analysis, it is concluded that impact response of the of sand-filled aluminium honeycomb sandwich structure is under the influence of honeycomb material, geometric parameters, sand properties, packing density, sand-honeycomb interaction, impact energy and impactor velocity.

Under the impact of low energy level, the sand-filling could effectively enhance the strength and stiffness of the sandwich structures with a softer core. If the mass of the core was kept constant, it is better to select a smaller and shorter core for the structure. Under the impact of high energy level and at the fixed height of the core, the mid-span deflection of the structure would decrease when the core height reached a fixed value, and the damaged area was localized and shrunk to a hole at the center of the face sheet at full penetration.

The results simulated by the finite-element/SPH model are in good agreement with the experimental results, indicating that the proposed model can make reasonable predictions of the dynamic responses and damage modes of the structures under impact loads.

This research sheds new light on the theory and design of protective structure, and provides a meaningful reference to the multi-objective optimization for the sand-filled aluminium honeycomb sandwich structure.

References

1. I.T. Lee, Y. Shi, A.M. Afsar, Low velocity impact behavior of aluminum honeycomb structures, 2010, AdvanceSd Composite Materials, vol. 19, no. 1, pp. 19-39.
2. G. Belingardi, P. Martella, L. Peroni, Fatigue analysis of honeycomb-composite sandwich beams, 2007, Composites Part A Applied Science & Manufacturing vol. 38, no. 4, pp. 1183-1191.
3. A. Akatay, M.Ö. Bora, O. Çoban, The influence of low velocity repeated impacts on residual compressive properties of honeycomb sandwich structures, 2015, Composite Structures, vol. 125, pp. 425-433.
4. J.S. Yang, L. Ma, R. Schmidt, Hybrid lightweight composite pyramidal truss sandwich panels with high damping and stiffness efficiency, 2016, Composite Structures, vol. 148, pp. 85-96.
5. G. Zhang, B. Wang, L. Ma, Energy absorption and low velocity impact response of polyurethane foam filled pyramidal lattice core sandwich panels, 2014, Composite Structures, vol. 108, pp. 304-310.

6. H. Wang, K.R. Ramakrishnan, K. Shankar, Experimental study of the medium velocity impact response of sandwich panels with different cores, 2016, Materials & Design, vol. 99, pp. 68-82.
7. R. Mohmmed, F. Zhang, B. Sun, Static and low-velocity impact on mechanical behaviors of foam sandwiched composites with different ply angles face sheets, 2014, Journal of Composite Materials, vol. 48, pp. 1173-1188.
8. T. Zhang, Y. Yan, J. Li, Low-velocity impact of honeycomb sandwich composite plates, 2015, Journal of Reinforced Plastics & Composites, vol. 35.
9. D. Wang, Z. Ba, Mechanical property of paper honeycomb structure under dynamic compression, 2015, Materials & Design, vol. 77, pp. 59-64.
10. B. Han, K. Qin, B. Yu, Honeycomb-corrugation hybrid as a novel sandwich core for significantly enhanced compressive performance, 2016, Materials & Design, vol. 93, pp. 271-282.
11. H. Mozafari, S. Khatami, H. Molatefi, out of plane crushing and local stiffness determination of proposed foam filled sandwich panel for Korean Tilting Train eXpress-Numerical study, 2015, Materials & Design, vol. 66, pp. 400-411.
12. S. Shi, Z. Sun, X. Hu, Flexural strength and energy absorption of carbon-fiber–aluminum-honeycomb composite sandwich reinforced by aluminum grid, 2014, Thin-Walled Structures, vol. 84, pp. 416-422.
13. S.S. Shi, Z. Sun, X.Z. Hu, Carbon-fiber and aluminum-honeycomb sandwich composites with and without Kevlar-fiber interfacial toughening, 2014, Composites Part A Applied Science & Manufacturing, vol. 67, pp. 102-110.
14. C. Wang, R.Q. Liu, Z.Q. Deng, Experimental and numerical studies on aluminum honeycomb structure with various cell specifications under impact loading, 2008, Journal of Vibration and Shock, pp. 121-126.
15. J. Zhang, M.F. Ashby, The out-of-plane properties of honeycombs, International Journal of Mechanical Sciences, vol. 34, no. 6, pp. 475-489.
16. G.W. Zhao, J.Q. Bai, Y.F. Qi, Average plastic collapse stress model of metallica honeycomb structure under out-of-plane impact load, 2016, Journal of Vibration and Shock, vol. 35, pp. 50-54.
17. M. Omidvar, M. Iskander, and S. Bless, Response of granular media to rapid penetration, 2014, International Journal of Impact Engineering, vol.66, no. 4, pp. 60-82.